Polarity switching from p- to n-type in a single thermoelectric donor-acceptor copolymer by p-type doping

Jing Wang
Xi'an Jiaotong University
Yizhuo Wang
Xi'an Jiaotong University
Qing Li
Xi'an Jiaotong University
Zhanchao Li
Xi'an Jiaotong University
Liqing Xu
Xi'an Jiaotong University
Kuncai Li
Xi'an Jiaotong University
Hong Wang (hong.wang@xjtu.edu.cn)
Xi'an Jiaotong University https://orcid.org/0000-0002-7989-1672

Letter

Keywords: Polarity switching, Donor-acceptor copolymer, Thermoelectric, Organic diode, P-type doping.

Posted Date: February 3rd, 2021

DOI: https://doi.org/10.21203/rs.3.rs-189287/v1

Polarity switching from p- to n-type in a single thermoelectric donor-acceptor copolymer by p-type doping

Jing Wang[1], Yizhuo Wang[1], Qing Li[1], Zhanchao Li[1], Liqing Xu[1], Kuncai Li[1],Hong Wang[1,2]*,

[1]Frontier Institute of Science and Technology, Xi'an Jiaotong University, Xi'an, 710054, China

[2]State Key Laboratory of Multiphase Flow in Power Engineering, Xi'an Jiaotong University, Xi'an, 710054, China

E-mail: hong.wang@xjtu.edu.cn

Abstract

The transport mechanism of organic materials is still far away from being well understood and controlled although conducting polymers have been discovered since 1977. It is rare to see conducting polyers possessing high bipolar (p- and n-type) electrical conductivities within a single bulk doped organic polymer without the assistant of gate voltage. Here, we report a novel approach to provide high performance n-type materials by p-type doping. More importantly, the bipolar electrical conductivities of the donor-acceptor conducting polymer are high, resulting high bipolar power factors among the solution-processable ambipolar D-A copolymers. A fully organic p-n junction is created in a planar film, exhibiting a high rectification ratio of 2 x 10^2 at $\pm$5 V with a high current density of 3 A/cm^2. Structural and spectroscopic tests have been performed to provide a fundamental understanding of the polarity switching mechanism. The results open the opportunity of making p- and n-type modules with a single conducting polymer for future modern organic electronics.

Keywords: Polarity switching; Donor-acceptor copolymer; Thermoelectric; Organic diode; P-type doping.

Introduction

Conducting polymers have the potential advantages of lower manufacturing cost by using traditional printing techniques to produce electronic modules at a large scale,[1] which makes them very attractive for innovative electronic applications, especially for flexible electronic devices.[2, 3] Large progress has been achieved in developing functional conducting polymers in many fields such as organic thermoelectrics,[1, 2, 4] organic solar cells,[1] organic field-effect transistors[5] and organic light-emitting diodes,[6] *etc* since the conducting polymer was discovered for the first time by Heeger, MacDiarmid, and Shirakawa in 1977.[7] However, the transport of holes and electrons in conducting polymers is still far away from being well understood and controlled.

Making p- and n-type modules with a single conducting polymer is still very challenging for organic materials although it can be easily realized for inorganics such as doping silicon with phosphorus and boron to make n-type and p-type semiconductors, respectively. For modern organic electronics, p-type and n-type materials are equally important and desired. Making p- and n-type modules with a single conducting polymer would simplify the fabrication processes of organic devices with large scalability and low cost by combining with traditional printing techniques to pattern a single conducting polymer with p- and n-type dopants. Besides, it may improve the performance of organic devices. For example, Roncali suggested that single material solar cells would be the next frontier for organic photovoltaics since they would have a longer lifetime due to the strong stabilization of the morphology of the interface.[8, 9] Toffanin and co-workers reported that single-layer light-emitting transistors might ensure good charge transport together with an efficient light-emission in the solid-state.[10] Wang and Yu *et. al.* reported that a novel organic Schottky barrier diode created in a single planar polymer film exhibited a remarkable current density of 30 A/cm^2 that is 2-3 orders in magnitude higher superior to that of previously reported organic materials.[6] Because it excluded interfaces that generally exist between p- and n-type modules, resulting in smooth current flow and subsequently improving the performance of the devices. These promising results of single material devices light the enthusiasm in making p- and n-type modules with a single conducting polymer.

However, not many conducting polymers can transport both holes and electrons. In general, the carrier polarity of a conducting polymer strongly depends on its molecular structure. Once a conducting polymer is synthesized, it may prefer to transport either electrons or holes. The majority of the conducting polymers exhibit unipolar transport property, which can only transport either holes or electrons. In contrast, ambipolar conducting polymers exhibiting both positive and negative Seebeck coefficient were reported in very limited cases.[4, 11, 12, 13] Especially, it is very challenging to achieve conducting polymers with high bipolar electrical conductivities (possessing high electrical conductivity for both p- and n-type).

Currently, the popular strategy to make ambipolar conducting polymer is to co-polymerize electron-rich groups (donors, D) and electron-deficient groups (acceptors, A).[14, 15, 16] However, only a small portion of the donor-acceptor copolymers successfully exhibited bipolar transport properties.[17, 18, 19] Although D-A copolymers have been reported to have very high motilities over 20 $cm^2/(V{\cdot}s)$ recently,[19, 20] the electrical conductivity for the D-A copolymers are often in the range of 10^{-3} – 10^{-5} S/cm.[21, 22] These ambipolar conducting polymers with low electrical conductivities are mainly used in organic field-effect transistors (FETs) or organic solar cells. Moreover, most of these ambipolar conducting polymers exhibit bipolar electrical conductivities in FET devices that require the assistant of a gate voltage.[23] Very rare examples were reported to have bipolar electrical conductivities for bulk-doped conducting polymers without the assistant of the gate voltage.[19, 24] To the best of our knowledge, bipolar electrical conductivities over 10^{-2} S/cm have never been reported for D-A copolymers up to date.

Here, we report that a solution-processable D-A copolymer poly (2,5-bis(2-octyldodecyl)-3,6-di(thiophen-2-yl)diketopyrrolo[3,4-c]pyrrole-1,4-dione-alt-thieno[3,2-b]thiophen) (DPPTTT, shown in Figure 1) can have high bipolar electrical conductivities after being doped by $FeCl_3$ ($DPPTTT_{FeCl3}$). It exhibits the highest p-type electrical conductivity of 130.6 S/cm and a high n-type electrical conductivity of 14.2 S/cm superior to that of most of the solution-processable D-A copolymers (Table S1 and S2). The high electrical conductivity leads to a high p-type thermoelectric power factor of 23.4 $\mu W/(mK^2)$ as well as

a high n-type thermoelectric power factor of 0.66 μW/(mK^2), which are all the highest for p- and n-type solution-processable ambipolar D-A copolymers, respectively (Figure S7). The conversion mechanism was addressed after performing structural and spectroscopic tests. A p-n junction is created in a planar thin film, exhibiting a high rectification ratio of 2 x 10^2 at ±5 V for fully printed organic diodes, which further demonstrates the conversion of the p-type D-A copolymer to n-type. The rectification performance meets the requirement for high-frequency radio-frequency-identification (R-ID) tags.[25, 26] These results may open the opportunity for developing new organic electronic devices with a single organic material.

Results and discussion

Molecular structures of DPPTTT, poly(3-hexylthiophene) (P3HT) and the p-type dopants: F4TCNQ, PTS-Fe, CN6-CP (2,3,5,6-Tetrafluoro-7,7,8,8-tetracyanoquinodimethane, Iron p-toluenesulfanate, hexacyano-trimethylene-cyclopropane) are shown in Figure 1a. A solution-processable method was used to prepare DPPTTT and P3HT films on glass substrates as shown in Figure S1. Six commercially available p-type dopants were studied at the same molar doping ratio (MDR = 1, repeat units: dopant ratio of 1: 1). Pristine DPPTTT is almost an insulator with a poor electrical conductivity that is not measurable. Its electrical conductivity increases after being doped. The electrical conductivities are in the order of $\sigma_{FeCl3} > \sigma_{CN6\text{-}CP} > \sigma_{PTS\text{-}Fe} > \sigma_{CuCl2} > \sigma_{F4TCNQ} > \sigma_{Fe2(SO4)3}$. The trend is mainly related to the doping ability of the p-type dopants. For example, CN6-CP has a lower the lowest unoccupied molecular orbital (LUMO) of -5.87 eV than F4TCNQ (LUMO = -5.24 eV),[27] which lead to the higher electrical conductivity of DPPTTT$_{CN6\text{-}CP}$ than DPPTTT$_{F4TCNQ}$. DPPTTT$_{FeCl3}$ shows the highest p-type electrical conductivity among the six p-type dopants which may be due to the small size and high electron affinity of $FeCl_3$ as reported in previous literature.[28]

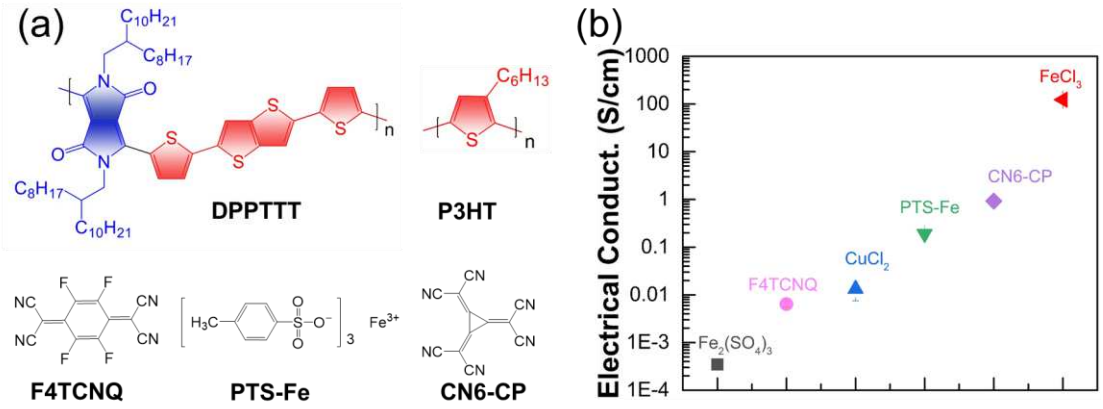

Figure 1 (a) Molecular structure of the polymers (DPPTTT and P3HT) and the six commercially available dopants. (b) Electrical conductivities of DPPTTT after p-type doped at MDR=1.

Electrical conductivity and Seebeck coefficient of DPPTTT doped with $FeCl_3$ at different concentrations were measured at room temperature as shown in Figure 2. The electrical conductivity of $DPPTTT_{FeCl3}$ increases with the raise of $FeCl_3$ concentration until it reaches the maximum of 130.6 S/cm at the $FeCl_3$ concentration of 21 wt.%. Then the electrical conductivity decreases while further increasing the concentration of $FeCl_3$. Scanning electron microscopy (SEM) was performed to understand the electrical conductivity drop from the $FeCl_3$ concentration of 21 wt.%. Figure 2d, 2e and 2f show the SEM images of pristine DPPTTT, $DPPTTT_{FeCl3\text{-}21wt.\%}$, and $DPPTTT_{FeCl3\text{-}84wt\%}$, respectively. Pristine DPPTTT film is composed of continuous agglomerates with the size of ~50 x 50 nm (Figure 3a and 3d). After by doped $FeCl_3$, the agglomerates aggregate as shown in the SEM images[29] of $DPPTTT_{FeCl3\text{-}21wt.\%}$ (Figure 3b and 3e) and $DPPTTT_{FeCl3\text{-}84wt.\%}$ (Figure 3c and 3f). The gaps between the agglomerates increase because of the aggregation, which may be one of the main reasons for the decrease of electrical conductivity from $FeCl_3$ concentration of 21 wt.% in Figure 2a. Atomic force microscopy (AFM) was performed to identify the roughness of the film. As shown in Figure S2, the root mean square (RMS) [30] for pristine DPPTTT, $DPPTTT_{FeCl3\text{-}21wt.\%}$ and $DPPTTT_{FeCl3\text{-}84wt\%}$ are 2.95 nm, 4.47 nm, and 36.6 nm, respectively. It further confirms that the aggregation of DPPTTT agglomerates at high $FeCl_3$ concentration over 21 wt.%. Temperature dependence of the electrical

conductivity of DPPTTT$_{FeCl3\text{-}21wt.\%}$ and DPPTTT$_{FeCl3\text{-}84wt\%}$ at the temperature range of 150K-300K were performed as shown in Figure S3. The electrical conductivities increase with the increase of temperature, indicating that the charge transport in DPPTTT$_{FeCl3}$ fits the variable range hopping model as reported for most of the conducting polymers. The activation energy calculated from the plots are 43.64 meV and 81.44 meV for DPPTTT$_{FeCl3\text{-}21wt.\%}$ and DPPTTT$_{FeCl3\text{-}84wt\%}$, respectively. The larger activation energy should be due to the larger gaps between the agglomerates, leading to lower electrical conductivity of DPPTTT$_{FeCl3\text{-}84wt\%}$.

Figure 2b shows the Seebeck coefficient of DPPTTT$_{FeCl3}$ as a function of the $FeCl_3$ concentration. It is interesting to notice that the Seebeck coefficient of DPPTTT$_{FeCl3}$ switching from p- to n-type. Pristine DPPTTT is a p-type material according to previous works[28, 31, 32]. The Seebeck coefficient of DPPTTT$_{FeCl3\text{-}10wt\%}$ is +223 μV/K, which indicates that it is still p-type at low $FeCl_3$ concentration. The Seebeck coefficient decreases while more $FeCl_3$ is added, which is due to the increase of carrier concentration at a higher p-type doping level. However, the Seebeck coefficient of DPPTTT$_{FeCl3}$ becomes negative after the $FeCl_3$ concentration is over 47 wt.%. Further increasing the $FeCl_3$ concentration leads to more negative of the Seebeck coefficient. The negative Seebeck coefficient of DPPTTT$_{FeCl3}$ reveals that it becomes an n-type material. The maximum n-type electrical conductivity and the maximum Seebeck coefficient are 14.2 S/cm and -78.9 μV/K for DPPTTT$_{FeCl3\text{-}47wt\%}$ and DPPTTT$_{FeCl3\text{-}84wt\%}$, respectively.

The maximum p- and n-type electrical conductivities of DPPTTT$_{FeCl3}$ are compared with those of previously reported solution-processable D-A copolymers as shown in Table S1 and Table S2. Very rare examples were reported to have bipolar electrical conductivities for bulk-doped conducting polymers without the assistant of the gate voltage.[19, 24] High electrical conductivities over 2 S/cm for both p- and n-type in a single conducting polymer have never been reported in previous literature. Figure 2c shows the comparison of the maximum p- and n-type electrical conductivities of DPPTTT$_{FeCl3}$ with those of solution-processable D-A copolymers. To the best of our knowledge, the achieved maximum p- and n-type electrical conductivities

are the highest for p- and n-type solution doped D-A polymers. A few post doped solution-processable D-A polymers were reported recently to have higher electrical conductivities. Therefore, in comparison to all the solution-processable D-A polymers, the maximum p-type electrical conductivity of 130.6 S/cm for $DPPTTT_{FeCl3}$ is among the top 7 values of solution-processable state-of-the-art D-A copolymers reported in previous literature (including unipolar and ambipolar D-A polymers) (Table S1). The maximum n-type electrical conductivity of 14.2 S/cm for $DPPTTT_{FeCl3}$ is one of the best n-type electrical conductivities since only one example was reported previously to have higher n-type electrical conductivities over 14.2 S/cm (Table S2). Compared with previously reported ambipolar D-A copolymers, the maximum bipolar electrical conductivities are ~4-5 orders of magnitude higher than previously reported values. The high bipolar electrical conductivities indicate a potential way to make p- and n-type modules for modern organic electronics with a single conducting polymer, which may promote the revolution in the field of semiconducting polymers.

Electrical conductivity and Seebeck coefficient of $FeCl_3$ doped P3HT were measured at room temperature for comparison as shown in Figure 2. The electrical conductivity increases with the increase of $FeCl_3$ concentration, which reaches its maximum of 63 S/cm at the $FeCl_3$ concentration of 47 wt.% (Figure 2a). Then it starts to drop when further increasing the $FeCl_3$ concentration. The Seebeck coefficient of P3HT at the $FeCl_3$ concentration of 10 wt.% is +157 μV/K. It drops with the raising of the $FeCl_3$ concentration. Different from $FeCl_3$ doped DPPTTT, no switching from p- to n-type was observed. All the Seebeck coefficients for $P3HT_{FeCl3}$ samples are positive.

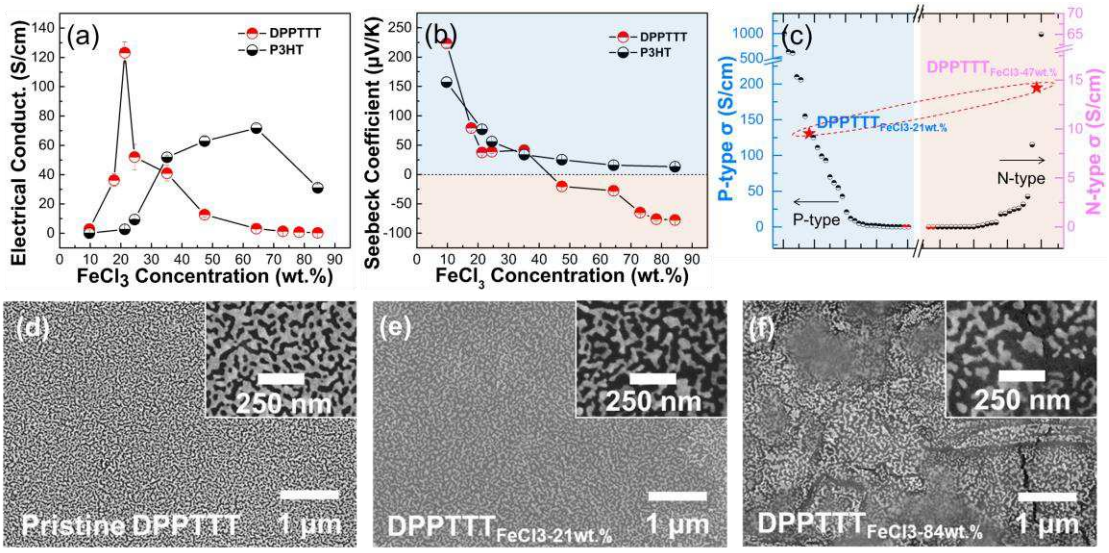

Figure 2 Electrical conductivity (a) and Seebeck coefficient of DPPTTT and P3HT as a function of $FeCl_3$ concentration. (c) Comparison of the maximum p- and n-type electrical conductivity of $DPPTTT_{FeCl3}$ with those solution-processable D-A copolymers. SEM images of pristine DPPTTT (d), $DPPTTT_{FeCl3\text{-}21wt.\%}$ (e), and $DPPTTT_{FeCl3\text{-}84wt.\%}$ (f).

Ultra-violet-visible near-infrared spectrophotometer (UV-vis-NIR) was performed to monitor the doping process of DPPTTT and P3HT. Figure 3a shows the UV-vis-NIR spectra of $DPPTTT_{FeCl3}$ films at different $FeCl_3$ concentration. A major peak appears at 810 nm for pristine DPPTTT film, which is assigned to the π-π^* transition of the DPP unit.[33, 34, 35] The major peak decreases together with the increase of a new broad peak at the near-infrared region when the $FeCl_3$ concentration increases. The decrease of the major peak should be due to the reduction of the neutral state of DPP units, which are converted into polaron state or bipolaron state[36] that result in the increase of the new peak at the near-infrared region. Figure 3d shows a clear conversion process of P3HT between the neutral state, the polaron state, and the bipolaron state. The neutral state of P3HT can be converted to the polaron state, which may be further converted to bipolaron state[37, 38]. At low $FeCl_3$ concentration, the neutral state P3HT was converted into the polaron state P3HT and bipolaron state P3HT, leading to the decrease of the neutral state peak at 532 nm, the increase of the polaron state peak at 832 nm, and the bipolaron state peak in the near-infrared region. At high $FeCl_3$ concentration, the decrease of polaron state peak at 832 nm indicates that the speed of polaron state P3HT converted to the bipolaron state is higher than that of polaron state P3HT generated. The

band gaps obtained from the UV-vis-NIR spectra of pristine DPPTTT and P3HT were 1.28 eV and 1.9 eV (Figure S4), respectively, which are consistent with previously reported works[39, 40, 41, 42, 43, 44].

The highest occupied molecular orbitals (HOMOs) of DPPTTT and P3HT were estimated by using the cyclic voltammetry (CV) method with a three-electrode electrochemical system. Ferrocene was used as the internal reference (see detailed description in the Supporting information). Figure 3b and 3e show that the oxidation peak edges (φ_{ox}) are 0.97 V and 0.94 V for DPPTTT and P3HT, respectively. Therefore, the HOMOs (E_{HOMO}) are -5.19 eV and -5.16 eV for DPPTTT and P3HT, respectively, according to the following equation[39]:

$$E_{HOMO} = -(4.8 - E_{1/2Ferrocene} + \varphi_{ox}) \quad (1)$$

where $E_{1/2Ferrocene}$ is the average of the oxidation peak potential and the reduction peak of the internal reference, ferrocene (shown in Figure S5). The obtained HOMO values are similar with the reported values in previous literature, -5.2 eV for P3HT[39, 45] and -5.2 eV for DPPTTT[43, 46, 47]. The LUMO values for DPPTTT and P3HT were calculated based on the CV results and the optical band gap to be -3.91 eV and -3.26 eV, respectively.

Ultraviolet photoelectron spectroscopy (UPS) was performed to provide the work function changes of DPPTTT and P3HT during the $FeCl_3$ doping process. Figure 3c shows UPS results of pristine DPPTTT, $DPPTTT_{FeCl3\text{-}21wt.\%}$, and $DPPTTT_{FeCl3\text{-}84wt.\%}$ along with that of gold as a reference. Their work functions (*WF*) can be obtained from the below equation[6]:

$$WF = hv + |E_f| - |E_{cutoff}| \quad (2)$$

where E_f and E_{cutoff} are respectively high and low kinetic energy cutoff, and hv is the photon energy of the used He I source (21.2 eV). The work function for pristine DPPTTT is achieved to be 4.58 eV. After doped with $FeCl_3$ at the concentration of 21 wt.%, the work function becomes larger (≈ 5.09 eV), indicating p-type doping of DPPTTT. It further increases to 5.4 eV while the $FeCl_3$ concentration is 84 wt.%. The work function of P3HT also increases after $FeCl_3$ doping as shown in Figure 3f. The work functions for pristine P3HT,

$P3HT_{FeCl3\text{-}21wt.\%}$ and $P3HT_{FeCl3\text{-}84wt.\%}$ are in the order of $WF_{pristine\text{-}P3HT}$ (4.14 eV) < $WF_{P3HT\text{-}FeCl3\text{-}21wt.\%}$ (4.39 eV) < $WF_{P3HT\text{-}FeCl3\text{-}84wt.\%}$ (4.95 eV). As a comparison, the work function of pure gold was measured to be 5.27 eV (Figure S6), which is in the range of previously reported values, 5.0 eV-5.4 eV.[6, 48, 49, 50]

The electronic band diagrams of DPPTTT and P3HT during the $FeCl_3$ doping process are respectively shown in Figure 3g and 3h. The Fermi level was obtained from the above work function $WF = E_{vac} - E_F$ (E_{vac} is vacuum level which typically equals zero) since the work function represents the energy barrier required for an electron to move at the Fermi level to free space.[51] The Fermi level of pristine DPPTTT derived from the UPS results is -4.58 eV, which close to the middle of the HOMO and LUMO of pristine DPPTTT (-4.55 eV). The slight differences between these two values should be due to the doping of oxygen or other contaminants in the air. After doped by $FeCl_3$, The Fermi level shifts to E_F = -5.09 eV for $DPPTTT_{FeCl3\text{-}21wt.\%}$, which is close to the HOMO of DPPTTT (-5.19 eV), indicating heavily p-type doping of DPPTTT (Figure 3g). While the Fermi level for $P3HT_{FeCl3\text{-}21wt.\%}$ is -4.39 eV, which is still far from its HOMO of -5.16 eV. These results indicate that DPPTTT is easier to be doped as compared to P3HT at the same $FeCl_3$ concentration. This trend is consistent with the theoretical calculated ionization potential (IP) for DPPTTT (5.9 eV) and P3HT (8.1 eV). The lower IP suggests the better electron-giving ability,[52, 53] leading to the lower Fermi level at the same $FeCl_3$ concentration. When the $FeCl_3$ is 84 wt.%, the Fermi level for $DPPTTT_{FeCl3\text{-}84wt.\%}$ shifts to -5.40 eV, which is below the HOMO of DPPTTT. While the Fermi level for $P3HT_{FeCl3\text{-}84wt.\%}$ is -4.95 eV, which is still above the HOMO of P3HT (Figure 3h).

Based on these results, we believe that the polarity switching of DPPTTT films from p- to n-type is due to the crossing of Fermi level (E_F) from above the HOMO (valence band, E_v) to below the HOMO. The hopping model reported by Fritzsche was typically used to describe the charge carrier transport in conducting polymers.[54] For a p-type material, the Seebeck coefficient is described as:

$$S = -\frac{k_B}{q}\left(\frac{E_F - E_V}{k_B T}\right) \quad (3)$$

where k_B, q, and T are the Boltzmann constant, the electron charge, and the

absolute temperature. For a neutral conducting polymer, its E_F localizes at the middle of LUMO and HOMO. As shown in Figure 3g and 3h, the E_F of pristine DPPTTT and P3HT lies close to the middle of the HOMO and LUMO. When they were doped by the p-type dopant, $FeCl_3$, the E_F will shift to the HOMO. For example, the E_F for $DPPTTT_{FeCl3\text{-}21wt.\%}$ shifts about 0.51 eV to the HOMO and the E_F for $P3HT_{FeCl3\text{-}21wt.\%}$ shifts about 0.25 eV to the HOMO. The shift of E_F leads to the reduction of the distance between the E_F and E_V, which subsequently results in the decrease of the Seebeck coefficient according to equation (3) as shown in Figure 2b. The Seebeck coefficients for $DPPTTT_{FeCl3\text{-}21wt.\%}$ and $P3HT_{FeCl3\text{-}21wt.\%}$ are positive because q is negative and $E_F - E_V > 0$. For $DPPTTT_{FeCl3\text{-}84wt.\%}$, the E_F is shifted below the HOMO ($E_F - E_V < 0$), which results in a negative Seebeck coefficient of -78.92 μV/K. The polarity switching is rare for conducting polymers, which has only been observed in several other polymer semiconductors, such as D-A copolymer PNDI2TEG-2T[19] and PDPH[24] switching from n- to p-type when doped by n-DMBI, poly(pyridinium phenylene) switching from n- to p-type when highly reduced by an organic sodium salt[54]. In contrast, no polarity switching was observed for $P3HT_{FeCl3}$ under the same conditions. To the best of our knowledge, it is the first time to report that D-A copolymer switches from p- to n-type while doping by a p-type dopant. More importantly, $DPPTTTT_{FeCl3}$ exhibits high p-type electrical conductivity of 130.6 S/cm as well as a high n-type electrical conductivity of 14.2 S/cm. The high bipolar electrical conductivities result in great p- and n-type power factors of $DPPTTTT_{FeCl3}$ among the ambipolar D-A copolymers as shown in Figure S7. These results indicate that it is very possible to make single material organic devices with p- and n-type modules for modern organic electronics in the future as what has been realized in inorganic materials.

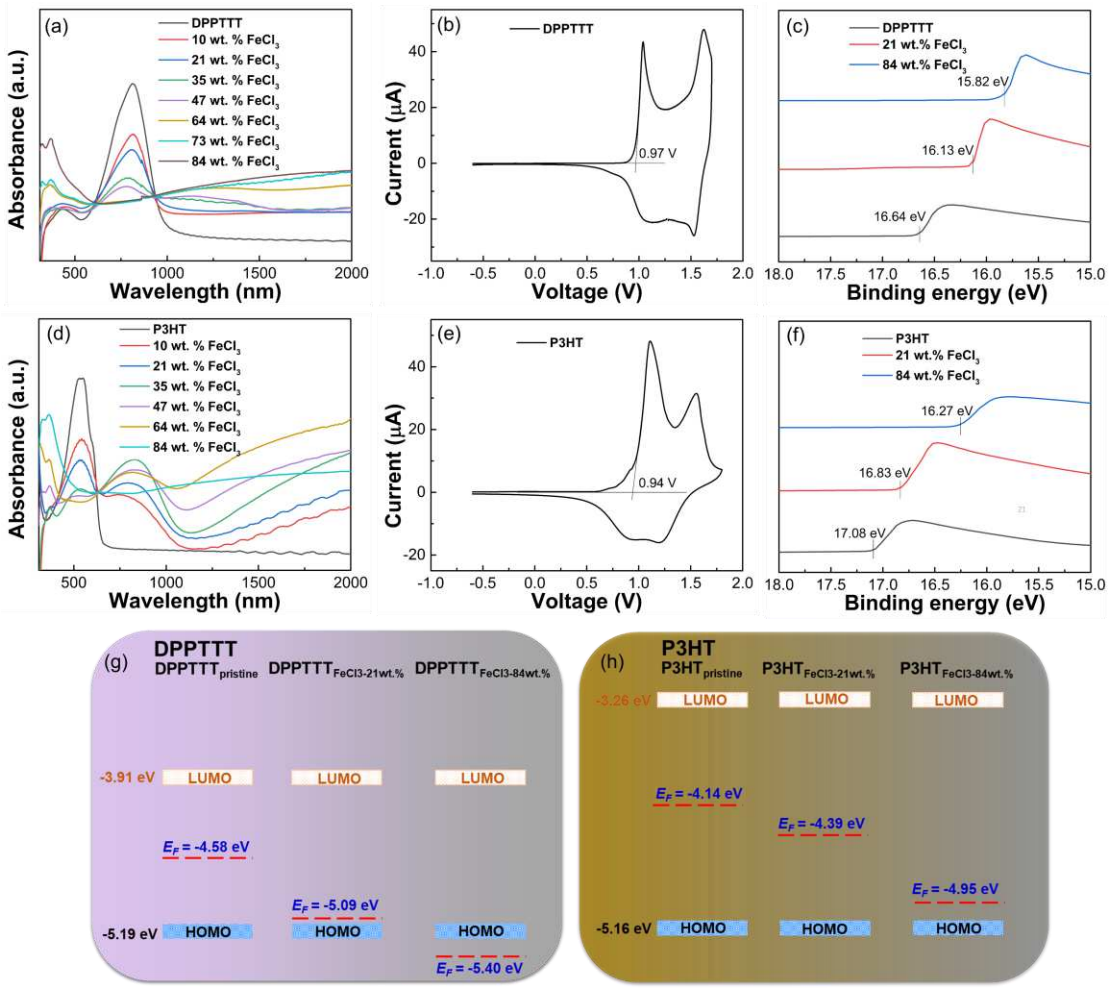

Figure 3 UV-vis-NIR spectra of DPPTTT (a) and P3HT (d) as a function of $FeCl_3$ concentration. The CV of pristine DPPTTT (b) and pristine P3HT (e). The UPS results for pristine DPPTTT, $DPPTTT_{FeCl3\text{-}21wt.\%}$, $DPPTTT_{FeCl3\text{-}84wt.\%}$ (c) and pristine P3HT, $P3HT_{FeCl3\text{-}21wt.\%}$, $P3HT_{FeCl3\text{-}84wt.\%}$ (f). The electronic band diagrams of DPPTTT (g) and P3HT (h) during the $FeCl_3$ doping process.

X-ray photoelectron spectroscopy (XPS) was performed to identify the change of the elements of DPPTTT during the p-type doping process. As shown in Figure 4a, the peak at 399.82 eV comes from N of DPP unit for pristine DPPTTT[55, 56, 57]. This peak shifted to 399.10 eV when the $FeCl_3$ concentration is 10 wt.%. A new peak at 400.97 eV appeared when the $FeCl_3$ concentration was increased to 21 wt.%. This new peak then shifted to 401.99 eV when the $FeCl_3$ concentration was further increased to 84 wt.%. The new peak is assigned to N^+, which was generated only at a high $FeCl_3$ concentration. The results indicate that TTT units were first oxidized at low $FeCl_3$ concentration and DPP units were oxidized at high $FeCl_3$ concentration. The changes of other

elements such as C 1S, O 1S, S 2p, Fe 2p, and Cl2p were shown in Figure S8. Based on the XPS results, the illustration of the molecular structure of doped DPPTTT is given in Figure 4d. The oxidation of DPPTTT will also lead to the color change of the films. As shown in Figure 4c, the color change from purple to gray was observed while increasing the concentration of $FeCl_3$. For the P3HT film, the color is dark gold, which changes gradually to dark grey as shown in Figure S9. A free-standing $DPPTTT_{FeCl3\text{-}84wt.\%}$ film was achieved by peeling off the thick film from a glass substrate. Figure 4b shows that the obtained film has good flexibility, which demonstrates the potential application of this material is flexible organic electronics.

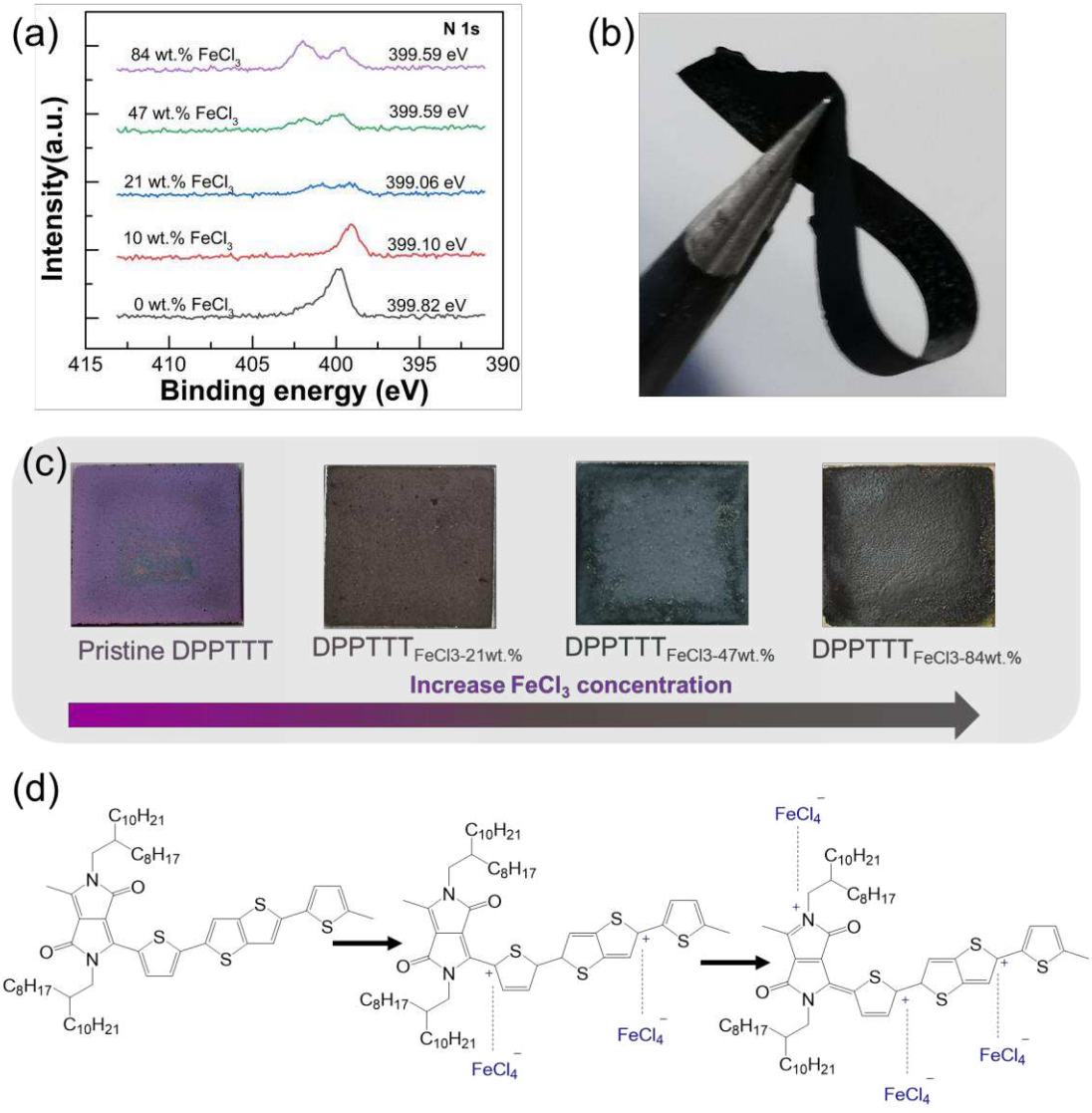

Figure 4 (a) XPS spectra and (b) optical images of DPPTTT at $FeCl_3$ concentration of 0

wt.%, 21 wt.%, 47 wt.%, 84 wt.%; (c) The molecular structure of DPPTTT before and after $FeCl_3$ doping.

The n-type $DPPTTT_{FeCl3}$ exhibited a modest stability in glovebox (O_2 < 0.2 ppm and H_2O < 0.02 ppm). Figure 5a shows that the electrical conductivity and the Seebeck coefficient of $DPPTTT_{FeCl3\text{-}84wt.\%}$ change with time. The Seebeck coefficient can be maintained after 25 days while the electrical conductivity can only be maintained for 7 days which drops to half of the electrical conductivity of fresh prepared $DPPTTT_{FeCl3\text{-}84wt.\%}$ after 15 days.

The sample preparation and testing environment were varied to study the effect of oxygen and water on its thermoelectric properties for $DPPTTT_{FeCl3\text{-}84wt.\%}$. The samples dried in a glovebox under the protection of N_2 were labeled as "N_2 (RH ≈ 0%)" in Figure 5b. The samples dried in a vacuum bucket filled with N_2 and O_2 with the RH ≈ 15% were labeled as "N_2 (RH ≈ 15%)" and "O_2 (RH ≈ 15%)", respectively. A high Seebeck coefficient of -78.9 μV/K was obtained for samples prepared under N_2 (RH ≈ 0%) which samples prepared under N_2 (RH ≈ 15%) and O_2 (RH ≈ 15%) shows poor Seebeck coefficients of -5.69 μV/K and -5.87 μV/K, respectively. The results indicate that water plays a major role in the drop of the n-type Seebeck coefficient. According to previous literature, both water and oxygen may affect the doping efficiency[58] since they will cause the degradation of the dopants as shown in the equation: $FeCl_4^- + H_2O + \frac{1}{2}O_2 \rightarrow Fe(OH)_2 + Cl_2 + e^-$. When the sample was dried in the air with a humidity of 65%, $DPPTTT_{FeCl3\text{-}84wt.\%}$ even shows a positive Seebeck coefficient, indicating that it is a p-type material. The variations in the electrical conductivity and Seebeck coefficient of $DPPTTT_{FeCl3\text{-}84wt.\%}$ are suggested to be related to the concentration of $FeCl_4^-$. When the sample was prepared in glovebox, the high $FeCl_4^-$ concentration will lead to the crossing of Fermi level from the position above the HOMO to a position below the HOMO, subsequently resulting in an n-type $DPPTTT_{FeCl3\text{-}84wt.\%}$. When a small portion of the $FeCl_4^-$ was degraded, the DPPTTT films contain both electrons and holes. Partial of the DPPTTT molecules maintained p-type will lead to the decrease of the n-type Seebeck coefficient of the entire film. At high humidity and oxygen conditions (in the air, RH ≈ 65%), the $DPPTTT_{FeCl3\text{-}84wt.\%}$ can only exhibit p-type

properties since the amount of p-type DPPTTT molecules become dominant. A post-treatment method has also been used to prepare $DPPTTT_{FeCl3}$ samples. The pristine DPPTTT samples were immersed in $FeCl_3$ solution with different concentrations. The electrical conductivities and the Seebeck coefficients of DPPTTT as a function of the $FeCl_3$ concentration are shown in Figure S10. However, no n-type Seebeck coefficient was obtained. The reason should be due to that no enough $FeCl_4^-$ was generated inside of the DPPTTT film since not many $FeCl_3$ can penetrate inside the DPPTTT films.

To identify the dominant carriers in the n-type $DPPTTT_{FeCl3\text{-}84wt.\%}$, the frequency-dependent (1-10^6 Hz) AC impedance was performed to distinguish electronic and ionic current.[4, 6] The n-type sample $DPPTTT_{FeCl3\text{-}84wt.\%}$ exhibited a deviation from a very high frequency (~ 10^6 Hz, Figure 5c), which is even higher than the deviation frequency of pristine DPPTTT (10^3 Hz). Typically, the deviation frequency for ionic conduction is about 0.3 Hz. The results suggest that electronic transport is dominant in the n-type material other than the ionic effect.[6]

Figure 5d shows a p-n junction made of p-type $DPPTTT_{FeCl3\text{-}21wt.\%}$ and n-type $DPPTTT_{FeCl3\text{-}84wt.\%}$. The sample was prepared by drop-casting p-type $DPPTTT_{FeCl3\text{-}21wt.\%}$ on half of the glass substrate first, and then drop-casting n-type $DPPTTT_{FeCl3\text{-}84wt.\%}$ on the other half of the glass substrate after the p-type film was dry (See Figure S11 in the supporting information). The current density was measured at room temperature as a function of the bias voltage in the range of -5 V–5 V with a scan rate of 0.5 V/s for $DPPTTT_{FeCl3\text{-}84wt.\%}$. The rectification was observed when a current was passed from the p-type side to the n-type side as shown in the inserted image and Figure 5d(1) (reverse bias). The forward bias (Figure 5d(2)) current density of the organic diode is 3.0 A/cm^2 at 5 V. A high rectification ratio (current density at 5 V divided by that of -5 V) was obtained to be ~2 x 10^2, which meets the requirement for high-frequency R-ID tags of rectification ratio > 100 at about 5 V.[25, 26] The current-voltage relations of single p-type $DPPTTT_{FeCl3\text{-}21wt.\%}$ and single n-type $DPPTTT_{FeCl3\text{-}84wt.\%}$ were measured for comparison. No rectification was obtained as shown in Figure S12.

The responses of a transient and steady-state current of the organic diode were measured while alternating input voltage of ±5 V. The reverse bias current was quickly recovered in less than 3 s to reach a steady-state by switching the bias polarity. The relaxation behavior should be due to the capacitive effects that may be derived from the high resistance of the films and dissociated ions by moisture. The quick response further indicates that this organic diode is electronic dominant since a typical ion-based organic diode is hard to maintain a steady current and requires a much longer time to reach a stationary current.[59, 60]

Kelvin probe techniques[6] were performed to identify the work function difference between the p-type $DPPTTT_{FeCl3\text{-}21wt.\%}$ side and the n-type $DPPTTT_{FeCl3\text{-}84wt.\%}$ side. Figure 5f shows the work function differences between the samples (WF_{sample}) and the probe tip (WF_{tip}), which is also called contact potential difference (CPD): $WF_{sample} = WF_{tip}$ - CPD. Assuming the work function of the used tip is 5.1 eV, the work functions for the p-type $DPPTTT_{FeCl3\text{-}21wt.\%}$ side and the n-type $DPPTTT_{FeCl3\text{-}84wt.\%}$ are 5.14 eV and 5.39 eV, respectively. The results match well with those values obtained by UPS as shown in Figure 3c, which further demonstrate the p- to n-type switching of DPPTTT by $FeCl_3$ doping.

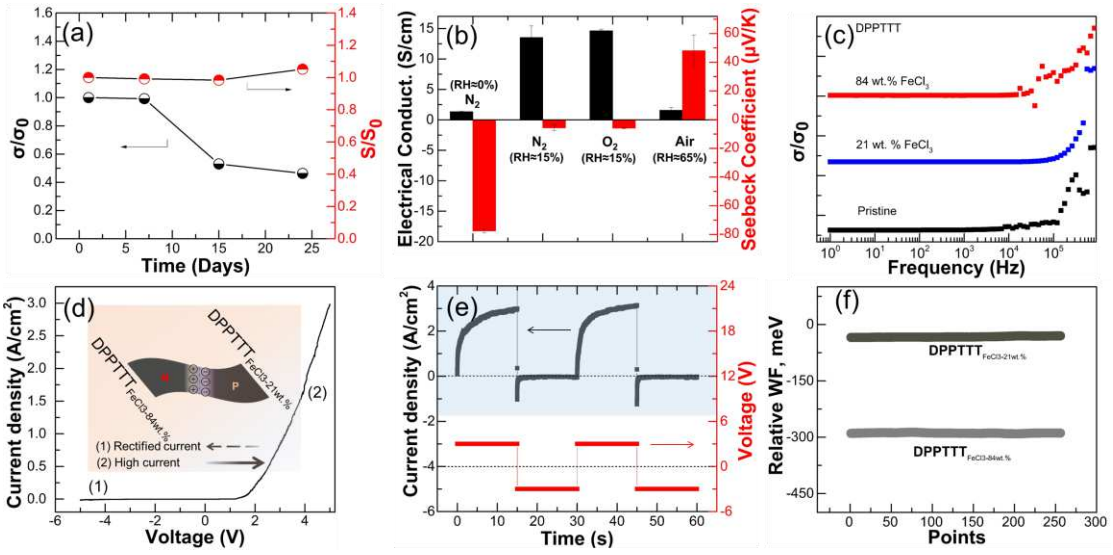

Figure 5 The electrical conductivity and the Seebeck coefficient of $DPPTTT_{FeCl3\text{-}84wt.\%}$ as a function of time (a) and varies with preparation conditions (b). (c) Freqency-dependent (1-

10^6 Hz) AC impedance of $DPPTTT_{FeCl3\text{-}84wt.\%}$. (d) Current of a p-n junction made of p-type $DPPTTT_{FeCl3\text{-}21wt.\%}$ and n-type $DPPTTT_{FeCl3\text{-}84wt.\%}$ as a function of bias voltage. (e) Transient and steady-state current of the organic diode. (f) CPD of p-type $DPPTTT_{FeCl3\text{-}21wt.\%}$ and n-type $DPPTTT_{FeCl3\text{-}84wt.\%}$ related to the probe tip.

Conclusion

We have demonstrated that solution-processable D-A copolymer can exhibit both high p- and n-type electrical conductivities over 10 S/cm during the p-type doping process. The polarity switching from p- to n-type is suggested to be due to the crossing of Fermi level from the position above HOMO to the position below the HOMO of the polymer as demonstrated by UPS, CV, KP, and UV-vis-NIR techniques. The high bipolar electrical conductivities are 4-5 orders of magnitude higher than those of previously reported ambipolar D-A copolymers, resulting in 4-5 orders of magnitude enhancement in the bipolar power factors among the solution-processable ambipolar D-A copolymers. These values are also among the top values of nowadays state-of-the-art solution-processable D-A copolymers including both unipolar and ambipolar D-A copolymers. A fully organic p-n junction was created with the p- and n-type material exhibiting a high rectification ratio of over 2 x 10^2 at $\pm$5 V with a high current density of 3 A/cm^2, which meet the requirement for high-frequency R-ID tags.[25, 26] The results open the opportunity of making p- and n-type modules with a single conducting polymer for future modern organic electronics.

Acknowledgment

H. W. acknowledges financial support from the National Natural Science Foundation of China (grant number: 51876151), the Fundamental Research Funds for the Central Universities, the World-Class Universities (Disciplines), and the Characteristic Development Guidance Funds for the Central Universities (grant number: PY3A010) and the start-up funding from Xi'an Jiaotong University (grant number: QY1J003). This work is also supported by the HPC platform and the Instrument Analysis Center, Xi'an Jiaotong University.

Conflicts of interest

There are no conflicts of interest to declare.

References

1. Zhang Z, Miao J, Ding Z, Kan B, Lin B, Wan X*, et al.* Efficient and thermally stable organic solar cells based on small molecule donor and polymer acceptor. *Nat Commun* 2019, **10**(1)**:** 3271.

2. Wang H, Yu C. Organic Thermoelectrics: Materials Preparation, Performance Optimization, and Device Integration. *Joule* 2019, **3**(1)**:** 53-80.

3. Wang H, Yi S-i, Pu X, Yu C. Simultaneously Improving Electrical Conductivity and Thermopower of Polyaniline Composites by Utilizing Carbon Nanotubes as High Mobility Conduits. *ACS Appl Mater Interfaces* 2015, **7**(18)**:** 9589-9597.

4. Wang H, Hsu J-H, Yi S-I, Kim SL, Choi K, Yang G*, et al.* Thermally Driven Large N-Type Voltage Responses from Hybrids of Carbon Nanotubes and Poly(3,4-ethylenedioxythiophene) with Tetrakis(dimethylamino)ethylene. *Adv Mater* 2015, **27**(43)**:** 6855-6861.

5. Liu Y-Y, Song C-L, Zeng W-J, Zhou K-G, Shi Z-F, Ma C-B*, et al.* High and Balanced Hole and Electron Mobilities from Ambipolar Thin-Film Transistors Based on Nitrogen-Containing Oligoacences. *J Am Chem Soc* 2010, **132**(46)**:** 16349-16351.

6. Wang H, Hsu J-H, Yang G, Yu C. Novel Organic Schottky Barrier Diode Created in a Single Planar Polymer Film. *Adv Mater* 2016, **28**(43)**:** 9545-9549.

7. Shirakawa H, Louis EJ, MacDiarmid AG, Chiang CK, Heeger AJ. Synthesis of electrically conducting organic polymers: halogen derivatives of polyacetylene, (CH). *Chem Commun* 1977(16)**:** 578-580.

8. Roncali J. Single Material Solar Cells: the Next Frontier for Organic Photovoltaics? *Adv Energy Mater* 2011, **1**(2)**:** 147-160.

9. Roncali J, Grosu I. The Dawn of Single Material Organic Solar Cells. *Adv Sci* 2019, **6**(1)**:** 1801026.

10. Prosa M, Moschetto S, Benvenuti E, Zambianchi M, Muccini M, Melucci M*, et al.* 2,3-thienoimide-ended oligothiophenes as ambipolar semiconductors for multifunctional single-layer light-emitting transistors. *J Mater Chem C* 2020.

11. Chiang CK, Gau SC, Fincher CR, Park YW, MacDiarmid AG, Heeger AJ. Polyacetylene, (CH)x: n-type and p-type doping and compensation. *Appl Phys Lett* 1978, **33**(1)**:** 18-20.

12. Koshida N, Wachi Y. Application of ion implantation for doping of polyacetylene films. *Appl Phys Lett* 1984, **45**(4)**:** 436-437.

13. Wada T, Takeno A, Iwaki M, Sasabe H, Kobayashi Y. Fabrication of a stable p–n junction in a polyacetylene film by ion implantation. *Chem Commun* 1985(17)**:** 1194-1195.

14. Shiyu FENG HL, Zekun LIU, Yahui LIU, Cuihong LI, Zhishan BO. Designing a High-Performance A-D-A Fused-Ring Electron Acceptor via Noncovalently Conformational Locking and Tailoring Its End Groups. *Acta Phys -Chim Sin* 2019, **35**(4)**:** 355-360.

15. Guoxiao JIA SZ, Liyan YANG,Chang HE,Huili FAN,Jianhui HOU. Development of Benzodithiophene-Based A-D-A Small Molecules with Different Acceptor End Groups for Efficient Organic Solar Cells. *Acta Phys -Chim Sin* 2019, **35**(1)**:** 76-83.

16. ZHAN X. A-D-A Small Molecular Electron Donors with Optimized End Groups for Efficient Organic Solar cells. *Acta Phys -Chim Sin* 2019, **35**(1)**:** 11-12.

17. Zaumseil J, Sirringhaus H. Electron and Ambipolar Transport in Organic Field-Effect Transistors. *Chem Rev* 2007, **107**(4)**:** 1296-1323.

18. Zhao Y, Guo Y, Liu Y. 25th Anniversary Article: Recent Advances in n-Type and Ambipolar Organic Field-Effect Transistors. *Adv Mater* 2013, **25**(38)**:** 5372-5391.

19. Yang J, Zhao Z, Wang S, Guo Y, Liu Y. Insight into High-Performance Conjugated Polymers for Organic Field-Effect Transistors. *Chem* 2018, **4**(12)**:** 2748-2785.

20. Yan H, Chen Z, Zheng Y, Newman C, Quinn JR, Dötz F*, et al.* A high-mobility electron-transporting polymer for printed transistors. *Nature* 2009, **457**(7230)**:** 679-686.

21. Schlitz RA, Brunetti FG, Glaudell AM, Miller PL, Brady MA, Takacs CJ*, et al.* Solubility-Limited Extrinsic n-Type Doping of a High Electron Mobility Polymer for Thermoelectric Applications. *Adv Mater* 2014, **26**(18)**:** 2825-2830.

22. Naab BD, Gu X, Kurosawa T, To JWF, Salleo A, Bao Z. Role of Polymer Structure on the Conductivity of N-Doped Polymers. *Adv Electron Mater* 2016, **2**(5)**:** 1600004.

23. Broch K, Venkateshvaran D, Lemaur V, Olivier Y, Beljonne D, Zelazny M*, et al.* Measurements of Ambipolar Seebeck Coefficients in High-Mobility Diketopyrrolopyrrole Donor–Acceptor Copolymers. *Adv Electron Mater* 2017, **3**(11)**:** 1700225.

24. Liu J, Ye G, Zee Bvd, Dong J, Qiu X, Liu Y*, et al.* N-Type Organic Thermoelectrics of Donor–Acceptor Copolymers: Improved Power Factor by Molecular Tailoring of the Density of States. *Adv Mater* 2018, **30**(44)**:** 1804290.

25. Ma L, Ouyang J, Yang Y. High-speed and high-current density C60 diodes. *Applied Physics Letters* 2004, **84**(23)**:** 4786-4788.

26. Pal BN, Sun J, Jung BJ, Choi E, Andreou AG, Katz HE. Pentacene-Zinc Oxide Vertical Diode with Compatible Grains and 15-MHz Rectification. *Advanced Materials* 2008, **20**(5)**:** 1023-1028.

27. Karpov Y, Erdmann T, Raguzin I, Al-Hussein M, Binner M, Lappan U*, et al.* High Conductivity in Molecularly p-Doped Diketopyrrolopyrrole-Based Polymer: The Impact of a High Dopant Strength and Good Structural Order. *Advanced Materials* 2016, **28**(28)**:** 6003-6010.

28. Liang Z, Zhang Y, Souri M, Luo X, Boehm AM, Li R*, et al.* Influence of dopant size and electron affinity on the electrical conductivity and thermoelectric properties of a series of conjugated polymers. *Journal of Materials Chemistry A* 2018, **6**(34)**:** 16495-16505.

29. Teng Y, Zhang Y, Heng L, Meng X, Yang Q, Jiang L. Conductive Polymer Porous Film with Tunable Wettability and Adhesion. *Materials* 2015, **8**(4)**:** 1817-1830.

30. Yoon SE, Shin SJ, Lee SY, Jeon GG, Kang H, Seo H*, et al.* Strategic Side-Chain Engineering Approach for Optimizing Thermoelectric Properties of Isoindigo-Based Conjugated Polymers. *Acs Applied Polymer Materials* 2020, **2**(7)**:** 2729-2735.

31. Zhang Q, Sun Y, Xu W, Zhu D. What To Expect from Conducting Polymers on the Playground of Thermoelectricity: Lessons Learned from Four High-Mobility Polymeric Semiconductors. *Macromolecules* 2014, **47**(2)**:** 609-615.

32. Jung IH, Hong CT, Lee U-H, Kang YH, Jang K-S, Cho SY. High Thermoelectric Power Factor of a Diketopyrrolopyrrole-Based Low Bandgap Polymer via Finely Tuned Doping Engineering. *Scientific Reports* 2017, **7**.

33. Sarkar T, Schneider SA, Ankonina G, Hendsbee AD, Li Y, Toney MF*, et al.* Tuning Intra and Intermolecular Interactions for Balanced Hole and Electron Transport in Semiconducting Polymers. *Chemistry of Materials* 2020, **32**(17)**:** 7338-7346.

34. Chen Z, Lee MJ, Shahid Ashraf R, Gu Y, Albert-Seifried S, Meedom Nielsen M*, et al.* High-Performance Ambipolar Diketopyrrolopyrrole-Thieno[3,2-b]thiophene Copolymer Field-Effect Transistors with Balanced Hole and Electron Mobilities. *Advanced Materials* 2012, **24**(5)**:** 647-652.

35. Li M, Balawi AH, Leenaers PJ, Ning L, Heintges GHL, Marszalek T*, et al.* Impact of polymorphism on the optoelectronic properties of a low-bandgap semiconducting polymer. *Nature Communications* 2019, **10**(1)**:** 2867.

36. Ding J, Liu Z, Zhao W, Jin W, Xiang L, Wang Z*, et al.* Selenium-Substituted Diketopyrrolopyrrole Polymer for High-Performance p-Type Organic Thermoelectric

Materials. *Angewandte Chemie-International Edition* 2019, **58**(52)**:** 18994-18999.

37. Gregory SA, Menon AK, Ye S, Seferos DS, Reynolds JR, Yee SK. Effect of Heteroatom and Doping on the Thermoelectric Properties of Poly(3-alkylchalcogenophenes). *Advanced Energy Materials* 2018, **8**(34).

38. Qu S, Yao Q, Yu B, Zeng K, Shi W, Chen Y*, et al.* Optimizing the Thermoelectric Performance of Poly(3-hexylthiophene) through Molecular-Weight Engineering. *Chemistry-an Asian Journal* 2018, **13**(21)**:** 3246-3253.

39. Lu J, Liang F, Drolet N, Ding J, Tao Y, Movileanu R. Crystalline low band-gap alternating indolocarbazole and benzothiadiazole-cored oligothiophene copolymer for organic solar cell applications. *Chemical Communications* 2008(42)**:** 5315-5317.

40. Eom Y, Song CE, Shin WS, Lee SK, Lim E. Rational design of pi-bridges for ambipolar DPP-RH-based small molecules in organic photovoltaic cells. *Journal of Industrial and Engineering Chemistry* 2017, **45:** 338-348.

41. Sun J, Yeh ML, Jung BJ, Zhang B, Feser J, Majumdar A*, et al.* Simultaneous Increase in Seebeck Coefficient and Conductivity in a Doped Poly(alkylthiophene) Blend with Defined Density of States. *Macromolecules* 2010, **43**(6)**:** 2897-2903.

42. Kim M, Ryu SU, Park SA, Choi K, Kim T, Chung D*, et al.* Donor-Acceptor-Conjugated Polymer for High-Performance Organic Field-Effect Transistors: A Progress Report. *Advanced Functional Materials* 2020, **30**(20).

43. Willems REM, Weijtens CHL, de Vries X, Coehoorn R, Janssen RAJ. Relating Frontier Orbital Energies from Voltammetry and Photoelectron Spectroscopy to the Open-Circuit Voltage of Organic Solar Cells. *Advanced Energy Materials* 2019, **9**(10).

44. Schroeder BC, Kurosawa T, Fu T, Chiu Y-C, Mun J, Wang G-JN*, et al.* Taming Charge Transport in Semiconducting Polymers with Branched Alkyl Side Chains. *Advanced Functional Materials* 2017, **27**(34).

45. Eom Y, Song CE, Shin WS, Lee SK, Lim E. Rational design of π-bridges for ambipolar DPP-RH-based small molecules in organic photovoltaic cells. *Journal of Industrial and Engineering Chemistry* 2017, **45:** 338-348.

46. Kim M, Ryu SU, Park SA, Choi K, Kim T, Chung D*, et al.* Donor–Acceptor-Conjugated Polymer for High-Performance Organic Field-Effect Transistors: A Progress Report. *Advanced Functional Materials* 2020, **30**(20)**:** 1904545.

47. Schroeder BC, Kurosawa T, Fu T, Chiu Y-C, Mun J, Wang G-JN*, et al.* Taming Charge Transport in Semiconducting Polymers with Branched Alkyl Side Chains. *Advanced*

Functional Materials 2017, **27**(34)**:** 1701973.

48. Koch N, Kahn A, Ghijsen J, Pireaux J-J, Schwartz J, Johnson RL*, et al.* Conjugated organic molecules on metal versus polymer electrodes: Demonstration of a key energy level alignment mechanism. *Applied Physics Letters* 2003, **82**(1)**:** 70-72.

49. Hu Q, Lu Z, Wang Y, Wang J, Wang H, Wu Z*, et al.* Double doping approach for unusually stable and large n-type thermoelectric voltage from p-type multi-walled carbon nanotube mats. *J Mater Chem A* 2020, **8**(26)**:** 13095-13105.

50. Wang Y, Lu Z, Hu Q, Qi X, Li Q, Wu Z*, et al.* Mass-produced metallic multiwalled carbon nanotube hybrids exhibiting high N-type thermoelectric performances. *Journal of Materials Chemistry A* 2021.

51. Kahn A. Fermi level, work function and vacuum level. *Materials Horizons* 2016, **3**(1)**:** 7-10.

52. Wang Y, Hao W, Huang W, Zhao H, Zhu J, Fang W. Tuning the Ambipolar Character of Copolymers with Substituents: A Density Functional Theory Study. *The Journal of Physical Chemistry Letters* 2020, **11**(10)**:** 3928-3933.

53. Kotadiya NB, Mondal A, Blom PWM, Andrienko D, Wetzelaer G-JAH. A window to trap-free charge transport in organic semiconducting thin films. *Nature Materials* 2019, **18**(11)**:** 1182-1186.

54. Hwang S, Potscavage WJ, Yang YS, Park IS, Matsushima T, Adachi C. Solution-processed organic thermoelectric materials exhibiting doping-concentration-dependent polarity. *Physical Chemistry Chemical Physics* 2016, **18**(42)**:** 29199-29207.

55. Shi K, Lu Z-Y, Yu Z-D, Liu H-Y, Zou Y, Yang C-Y*, et al.* A Novel Solution-Processable n-Dopant Based on 1,4-Dihydropyridine Motif for High Electrical Conductivity of Organic Semiconductors. *Advanced Electronic Materials* 2017, **3**(11).

56. Huang D, Yao H, Cui Y, Zou Y, Zhang F, Wang C*, et al.* Conjugated-Backbone Effect of Organic Small Molecules for n-Type Thermoelectric Materials with ZT over 0.2. *Journal of the American Chemical Society* 2017, **139**(37)**:** 13013-13023.

57. Yan X, Xiong M, Li J-T, Zhang S, Ahmad Z, Lu Y*, et al.* Pyrazine-Flanked Diketopyrrolopyrrole (DPP): A New Polymer Building Block for High-Performance n-Type Organic Thermoelectrics. *Journal of the American Chemical Society* 2019, **141**(51)**:** 20215-20221.

58. Lee S, Paine DC, Gleason KK. Heavily Doped poly(3,4-ethylenedioxythiophene) Thin Films with High Carrier Mobility Deposited Using Oxidative CVD: Conductivity Stability and Carrier Transport. *Advanced Functional Materials* 2014, **24**(45)**:** 7187-7196.

59. So J-H, Koo H-J, Dickey MD, Velev OD. Ionic Current Rectification in Soft-Matter Diodes with Liquid-Metal Electrodes. *Adv Funct Mater* 2012, **22**(3)**:** 625-631.

60. Cayre OJ, Chang ST, Velev OD. Polyelectrolyte Diode: Nonlinear Current Response of a Junction between Aqueous Ionic Gels. *J Am Chem Soc* 2007, **129**(35)**:** 10801-10806.

Figures

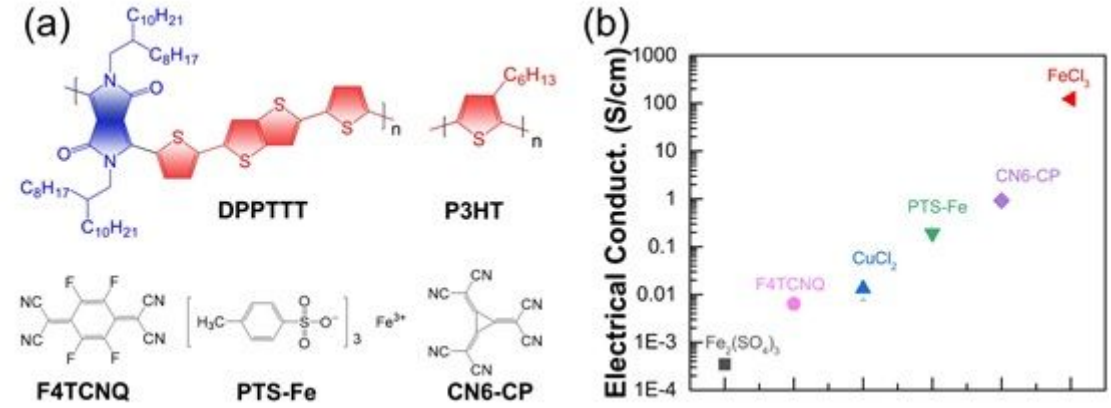

Figure 1

(a) Molecular structure of the polymers (DPPTTT and P3HT) and the six commercially available dopants. (b) Electrical conductivities of DPPTTT after p-type doped at MDR=1.

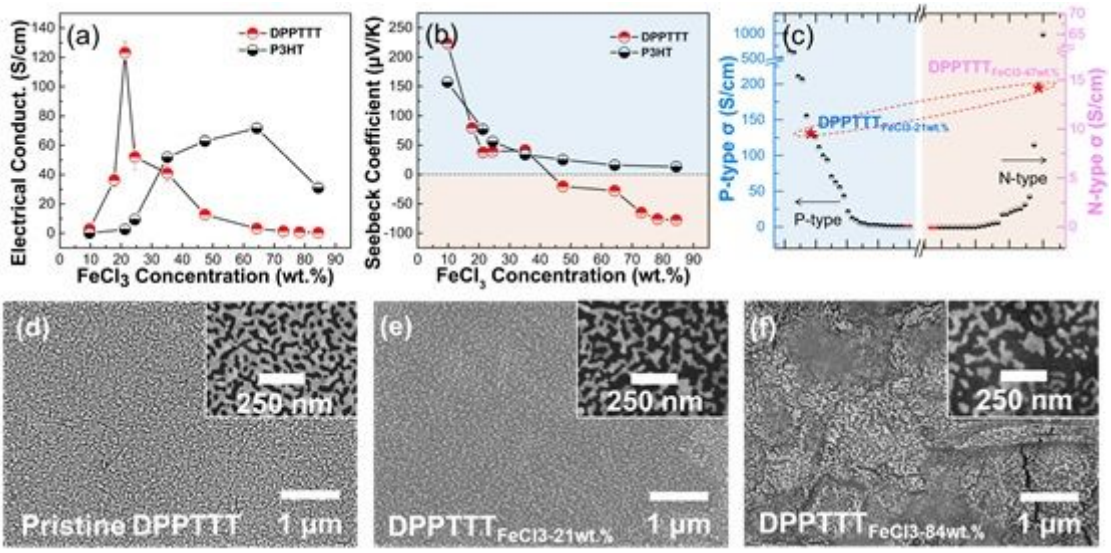

Figure 2

Electrical conductivity (a) and Seebeck coefficient of DPPTTT and P3HT as a function of FeCl3 concentration. (c) Comparison of the maximum p- and n-type electrical conductivity of DPPTTTFeCl3 with those solution-processable D-A copolymers. SEM images of pristine DPPTTT (d), DPPTTTFeCl3-21wt.% (e), and DPPTTTFeCl3-84wt.% (f).

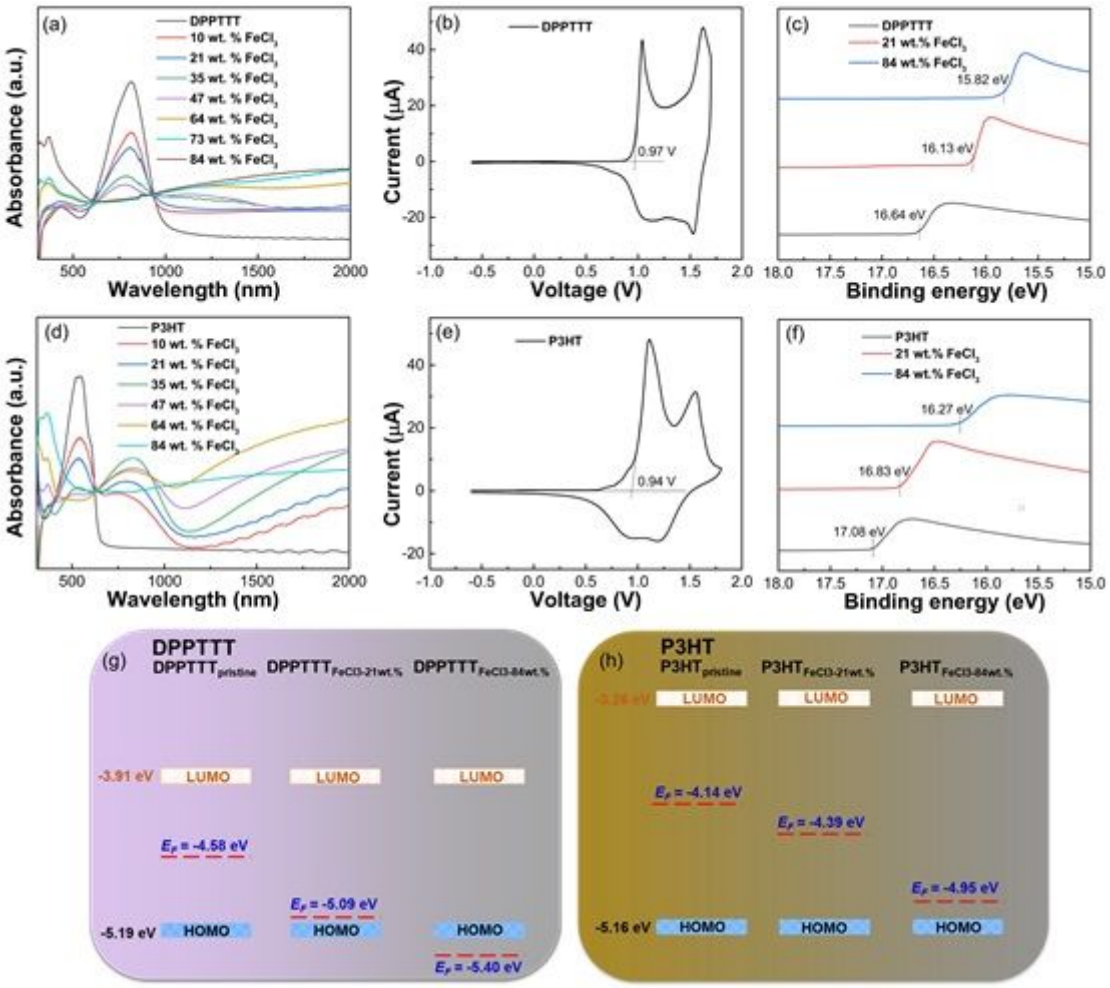

Figure 3

UV-vis-NIR spectra of DPPTTT (a) and P3HT (d) as a function of FeCl3 concentration. The CV of pristine DPPTTT (b) and pristine P3HT (e). The UPS results for pristine DPPTTT, DPPTTTFeCl3-21wt.%, DPPTTTFeCl3-84wt.% (c) and pristine P3HT, P3HTFeCl3-21wt.%, P3HTFeCl3-84wt.% (f). The electronic band diagrams of DPPTTT (g) and P3HT (h) during the FeCl3 doping process.

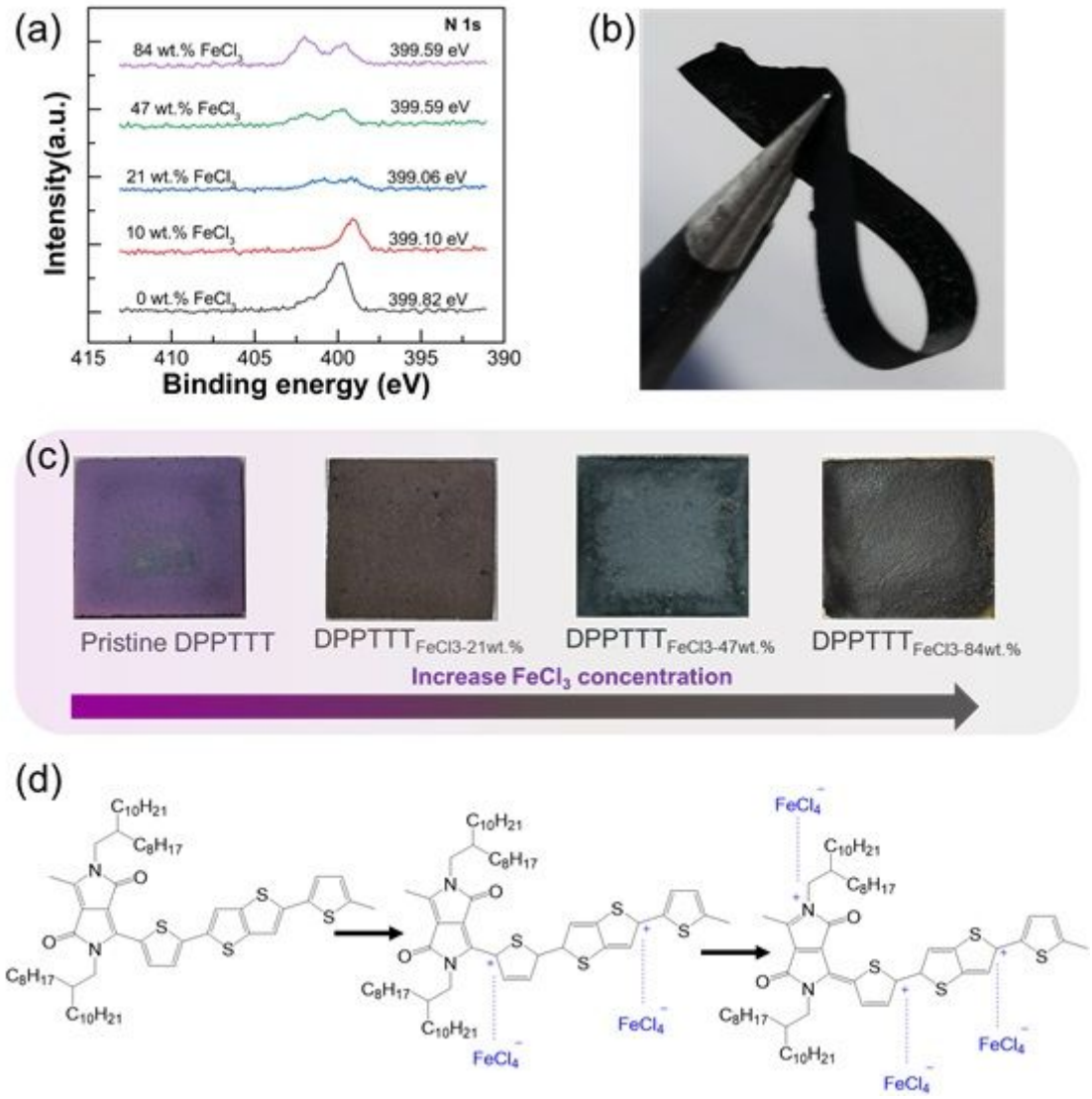

Figure 4

(a) XPS spectra and (b) optical images of DPPTTT at FeCl3 concentration of 0 wt.%, 21 wt.%, 47 wt.%, 84 wt.%; (c) The molecular structure of DPPTTT before and after FeCl3 doping.

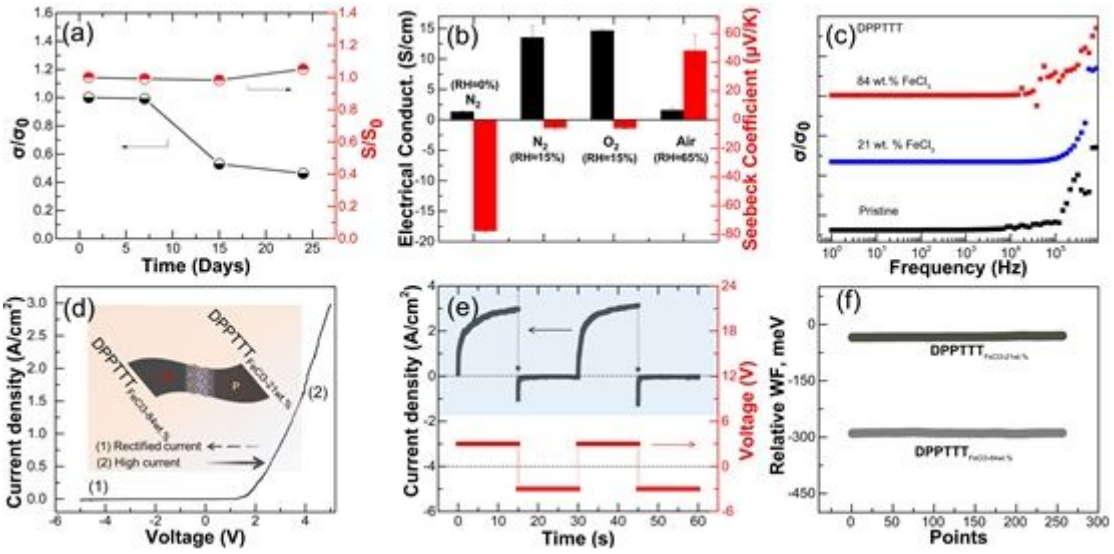

Figure 5

The electrical conductivity and the Seebeck coefficient of DPPTTTFeCl3-84wt.% as a function of time (a) and varies with preparation conditions (b). (c) Freqency-dependent (1-106 Hz) AC impedance of DPPTTTFeCl3-84wt.%. (d) Current of a p-n junction made of p-type DPPTTTFeCl3-21wt.% and n-type DPPTTTFeCl3-84wt.% as a function of bias voltage. (e) Transient and steady-state current of the organic diode. (f) CPD of p-type DPPTTTFeCl3-21wt.% and n-type DPPTTTFeCl3-84wt.% related to the probe tip.

Supplementary Files

This is a list of supplementary files associated with this preprint. Click to download.

- Supportinginfo.docx